GMR
The Original by FUNPEC-RP

Characterization of a complex chromosomal rearrangement in a girl with PURA syndrome

M.E. Minzhenkova[1], D.A. Yurchenko[1], N.A. Semenova[2], Z.G. Markova[1], A.A. Tarlycheva[1] and N.V. Shilova[1]

[1] Laboratory of Cytogenetics, Scientific department, Research Centre for Medical Genetics, Moscow, Russia
[2] Research and Counseling Department, Scientific department, Research Centre for Medical Genetics, Moscow, Russia

Corresponding author: M.E. Minzhenkova
E-mail: maramin@mail.ru

Genet. Mol. Res. 21 (4): gmr19065
Received May 24, 2022
Accepted August 22, 2022
Published October 06, 2022
DOI http://dx.doi.org/10.4238/gmr19065

ABSTRACT. Complex chromosomal rearrangements are extremely rare in humans. Most apparently balanced complex chromosomal rearrangements are *de novo*; they usually are detected in phenotypically normal subjects. Nevertheless, in some cases they are found in patients with multiple congenital abnormalities and neurodevelopmental disorders, which may be due to cryptic genomic imbalance. We report on a case of complex chromosomal rearrangement in a patient with an abnormal phenotype and neurodevelopmental delay. The conventional karyotyping of a child showed an apparently balanced three-way translocation t(4;7;5)(q31;p21;q31)dn. FISH and chromosomal microarray revealed that the rearrangement was far more complex than originally diagnosed, with more breakpoints involving chromosomes and four cryptic microdeletions on chromosomes 4 and 5. One copy number variant indicated microdeletion 5q31.3 syndrome associated with deletion/mutation of the gene *PURA*. A combination of several different approaches, including GTG, FISH and chromosomal microarrays, was sufficient to determine an unexpected level of

complexity and to resolve the nature of the complex chromosomal rearrangement.

Key words: Complex chromosomal rearrangement; PURA syndrome; FISH; Chromosomal microarray; Neurodevelopmental delay

INTRODUCTION

Complex chromosomal rearrangements (CCRs) are structural abnormalities characterized by more than one translocation with double or multiple rearrangements (Pai et al., 1980; Madan et al., 2012). Balanced chromosomal rearrangements are usually detected in phenotypically normal subjects. According to the literature, the majority of CCRs are de novo (about 70-75%) founded among patients with multiple congenital abnormalities and/or developmental delay (51%) and phenotypically normal subjects (49%) (Pellestor et al., 2011). Despite the relatively low incidence of CCRs in humans, the number of publications about CCRs will increase (Patsalis et al., 2004; Gu et al., 2008; Higgins et al., 2008; Aristidou et al., 2018). This can be explained by the expansion of diagnostic molecular and cytogenetic tools such as FISH, chromosomal microarray (CMA) and whole-genome sequencing (WGS).

More extensive studies of cases of patients with abnormal phenotype and apparently balanced translocations or CCRs detected by molecular genetic methods estimated that the most of the rearrangements associated with a cryptic imbalance. Some CCRs are more complex and almost all cases with abnormal phenotype are imbalanced (De Gregori et al., 2007; Sismani et al., 2008). A recent genome-wide-array study revealed that 90% of apparently balanced *de novo* CCRs have a cryptic deletion and/or duplication at the site of the breakpoints (Patsalis et al., 2004; De Gregori et al., 2007; Aristidou et al., 2018). Characterization of CCRs is important for the definition of their mechanisms of formation and their contribution to phenotype.

Here, we present a patient with an abnormal phenotype and neurodevelopmental abnormalities, and initially apparently balanced chromosomal rearrangement determined by GTG-banding. Molecular-cytogenetic methods revealed that apparent reciprocal translocation is in fact CCR, and there is a cryptic genomic imbalances associated with the breakpoints. Analysis of chromosomal microarray data has been useful in identifying of pathogenic CNV and disease associated genes. This case shares common features of profound hypotonia, developmental delay and white matter abnormalities on cerebral imaging.

MATERIAL AND METHODS

Cytogenetic analysis of the patient and her parents were performed on GTG-banded metaphase spreads obtained from cultured peripheral blood lymphocytes according to standard procedures. GTG-banded metaphase chromosomes were analyzed using Axio Imager A1 microscope (Carl Zeiss, Jena, Germany) with Ikaros Karyotyping System Software, V.5.8.14 (Metasystems, Altlussheim, Germany).

FISH was carried out using chromosomal preparations from cultured peripheral blood lymphocytes following the manufacturers' protocols. DNA probes for subtelomeric

regions of the short arm of chromosomes 7, the long arm of chromosome 4 (Sub-telomere 7pter, Sub-telomere 4qter, KREATECH, Amsterdam, The Netherlands), whole chromosome probe for the chromosome 4 and for the long arm of chromosome 5 (Whole Chromosome 4, Arm Specific long Probe 5; KREATECH, Amsterdam, The Netherlands), Satellite Enumeration Probe for chromosomes 5 and 7 (CEP 5 - SE 1/5/19; SE 7 (D7Z1), KREATECH, Amsterdam, The Netherlands). Multicolor Banding DNA probes on chromosomes 4, 5, 7, (XCyte Human mBAND probe; MetaSystems, Altlussheim, Germany) were applied. FISH results were analyzed using an AxioImager M.1 epifluorescence microscope (Carl Zeiss, Jena, Germany) and an Isis digital image processing software (MetaSystems, Altlussheim, Germany).

The CytoScan HD array (Affymetrix, Santa Clara, USA) was applied to detect the CNV across the entire genome following the manufacturer's protocols. Microarray-based copy number analysis was performed using the Chromosome Analysis Suite software version 4.0 (Thermo Fisher Scientific Inc.) and the results were presented on the International System for Human Cytogenomic Nomenclature 2020 (ISCN, 2020). Detected CNVs totally assessed by comparing them with published literature and the public databases: Database of Genomic Variants (DGV) (http://dgv.tcag.ca/dgv/app/home), DECIPHER (http://decipher.sanger.ac.uk/) and OMIM (http://www.ncbi.nlm.nih.gov/omim). Genomic positions refer to the Human Genome February 2009 assembly (GRCh37/hg19). The pathogenicity of variants evaluated according to the American College of Medical Genetics (ACMG) standard guidelines (Riggs et al., 2020).

A homemade DNA probes for chromosome 4 (regions 4q31.3 and 4q32.3) and chromosome 5 (region 5q31.2) were applied to characterize the structure of derivative chromosomes 4, 5, 7. Primers for the unique sequences of genes *TRIM2* (4q31.3 region), *TLL1* (4q32.3 region) and *SPOCK1* (5q31.2 region) were selected using the standard bioinformatics programs (BLAST), which are provided by the National Center for Biotechnological Information of the United States (NCBI) (Ye et al., 2012) and UCSC genome browser database (http://genome.ucsc.edu). All data are presented in the Supplementary Materials (Tables S1, S2, S3). Locus-specific DNA products were synthesized using long-range PCR by the BioMaster LR HS-PCR (2x) (BIOLABMIX LLC, Novosibirsk, Russia) on a GeneAmp PCR System 9700 (Applied Biosystems, California, USA) according to the manufacturer's protocols (http://www.biolabmix.ru). The derived oligonucleotides were labeled with Green 496 dUTP (the unique sequences of gene *TRIM2*), Red 580 dUTP (the unique sequences of genes *TLL1* and *SPOCK1*)(Enzo Life Sciences, Inc., NY, USA) by nick-translation and denatured at 75°C for 7 min. Chromosome slides were preincubated in 2SSC at 37°C for 45 min, denatured in 70% formamide/2SSC at 73°C for 3 min, and then dehydrated at -20°C in ethanol. Probe-hybridization mixture was applied on the chromosomes, incubated at 37°C for 16 h. Slides were washed three times in 4SSC, 0.1% Tween 20 at 45°C. The data were analyzed using the Isis software (MetaSystems, Altlussheim, Germany) and the epifluorescence microscope AxioImager M.1 (Carl Zeiss, Jena, Germany).

RESULTS

Case presentation

The patient, a girl three years old, was referred for karyotyping due to developmental delay. She was a first child of two healthy, unrelated parents. At 40 weeks of gestation, the delivery was normal; the Apgar scores of the neonate were 7/8. The birth weight was 3,210 g (-0.22 SD), length 50 cm (0.28 SD), and head circumference of 33 cm (-0.91 SD). Two hours after birth, she was transferred to neonatal intensive care with profound central nervous system depression, central apnea, and multifocal myoclonic seizures. She required mechanical ventilation for the first two weeks of life. From the birth, she had failed to thrive. Feeding was via nasogastric tube during a few months. Echocardiography was performed for the identification of ventricular septal defect in the muscular trabeculated septum.

At the age of three years, she had a developmental and speech delay. She had a profound hypotonia, abnormal seizure-like movements. She could not stay and sit. Multiple congenital anomalies included a microcephaly, a myopathic face, full cheeks, thick-arched eyebrows with synophrys, almond-shaped palpebral fissures, hypertelorism, epicanthus, and long eyelashes. She had asymmetric low set prominent ears, a flat nasal bridge, a short nose and a long philtrum, a small mouth, downturned corners of the mouth (Figure 1a, 1b), a high arched palate, camptodactyly, and arachnodactyly (Figure 1c).

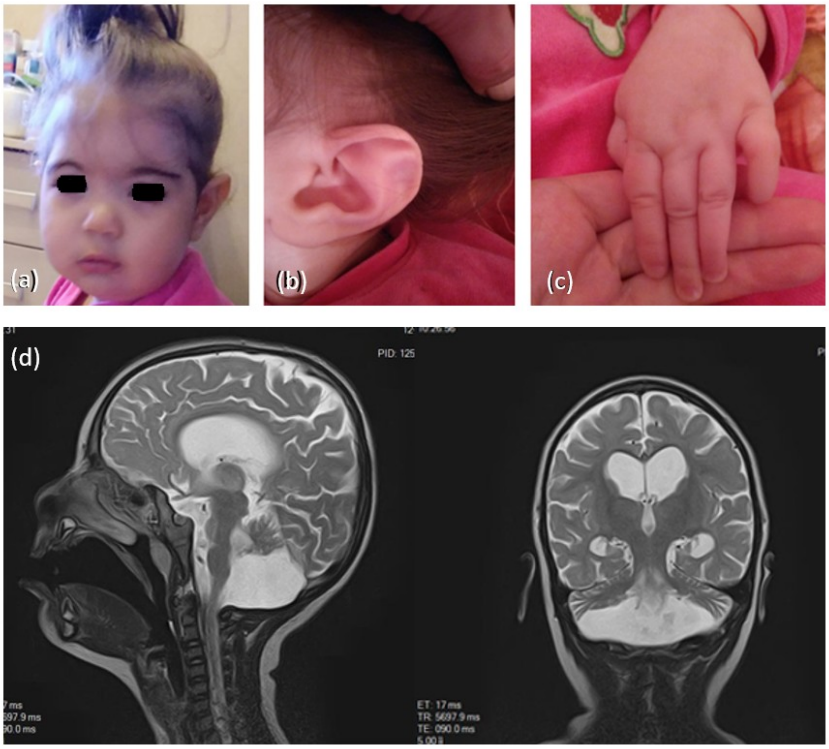

Figure 1. Patient presentation at age three years. (a) A myopathic face, thick arched eyebrows, almond-shaped palpebral fissures, a flat nasal bridge, a short nose and a long philtrum, full cheeks, micrognathia, a small mouth, downturned corners of the mouth; (b) Low set prominent ears; (c) Camptodactyly of the five fingers, arachnodactyly; (d) MRI shows hypoplasia of the corpus callosum and cerebellar vermis hypoplasia. The image demonstrates dilatation of the lateral ventricles and severely delayed myelination.

Electroencephalogram (EEG) revealed a diffuse encephalopathy. EEG video monitoring recorded discharges of epileptiform activity with a pre-dominance in the left posterotemporal region. The EEG also showed a mixture of focal/multifocal and regional epileptic discharges in the right posterotemporal region during sleep. However, the seizure-like clinical episodes were not associated with epileptiform discharges on video-EEG monitoring. The magnetic resonance imaging (MRI) of the brain at 3 years of age demonstrates hypoplasia of the cerebellum and corpus callosum, widening of the lateral ventricles and severely delayed myelination (Figure 1d).

Molecular - cytogenetic findings

GTG-banding analysis revealed an apparently balanced translocation between chromosomes 4, 5, 7 (Figure 2), whereas a normal karyotype was detected in the parents, indicating the *de novo* origin of the translocation. It is uncertain whether the break in the long arms of chromosomes 4, 5 is in regions q31, and in the short arm of chromosome 7 is in region p21.

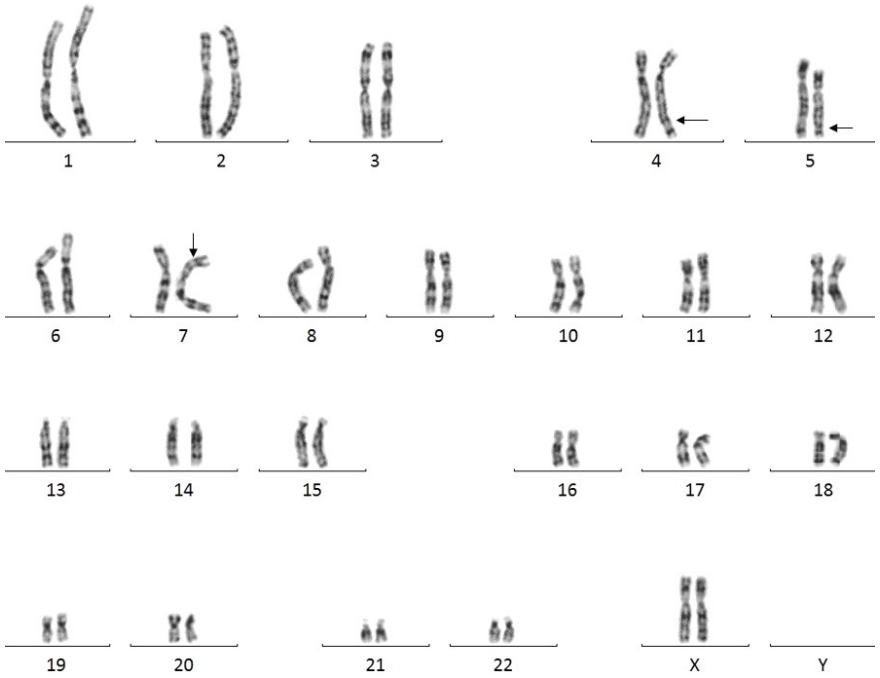

Figure 2. GTG banding of metaphase chromosomes. Karyotype 46,XX,t(4;7;5)(q?31;p?21;q?31)dn.

Multicolor Banding analysis of chromosomes 4, 5, 7 was employed to clarify a chromosomal rearrangement and to delineate the breakpoints in every chromosome (Figure 3). Unexpectedly, we detected that a segment of chromosome 4 was inserted into the long arm of derivative chromosome 5. Respectively, the present CCR classified by Madan as type III (Madan, 2012), because it implicated a number of breaks higher than the number of chromosomes involved and includes one insertion.

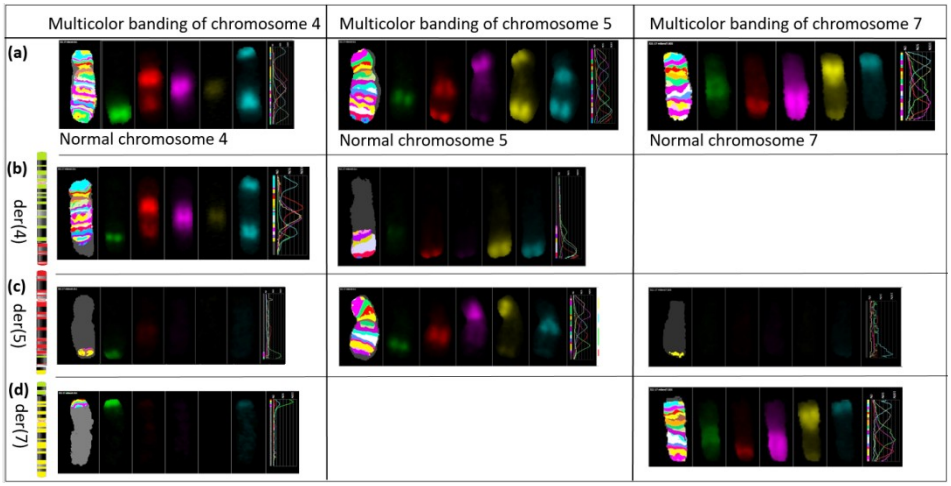

Figure 3. Multicolor banding (MCB) of chromosomes 4, 5, 7. MCB analyses evaluated hybridization profiles (signal intensity relative to the strongest signal on this chromosome) of corresponding fluorochromes: FITC, SpO, TR, Cy5, DEAC. (a) Normal homologues of chromosomes 4, 5, 7; (b) Derivative chromosome 4; (c) Derivative chromosome 5; (d) Derivative chromosome 7.

The analysis of MCB 4 and MCB 5 images of the abnormal chromosomes confirms that the false color showed produced in the terminal region of der(4) is a true chromosome 5 signal, and shows the MCB pattern interpreted derivative chromosome 4 as 4p16→4q31.2::5q31.2→5q35.3 (Figure 3b). MCB 4, MCB 5 and MCB 7 images of the abnormal chromosomes showed that the false color produced in the terminal region of der(5) is true chromosome 4 and chromosome 7 signals, and shows the MCB pattern interpreted derivative chromosome 5 as 5p15.3→5q31.1::4q32→4q34::7p21→7p22 (Figure 3c). MCB 4 and MCB 7 images of the abnormal chromosomes confirms that the false color produced in the terminal region of der(7) is true chromosome 4 signal. However, analyzing the hybridization profiles, we found that the fragment of chromosome 4 located on der(7) reflects different parts of chromosome 4. The proximal part of MCB 4 of der(7) contents low signal DEAC which should not be there (Figure 3d). Thereby, MCB pattern interpreted derivative chromosome 7 as 4q35→4q34::4q32→4q31.3::7p21→7q36. Whole Chromosome Painting, Arm-specific and Sub-Telomere probes were applied for confirming the complex chromosomal rearrangement (Figure 4).

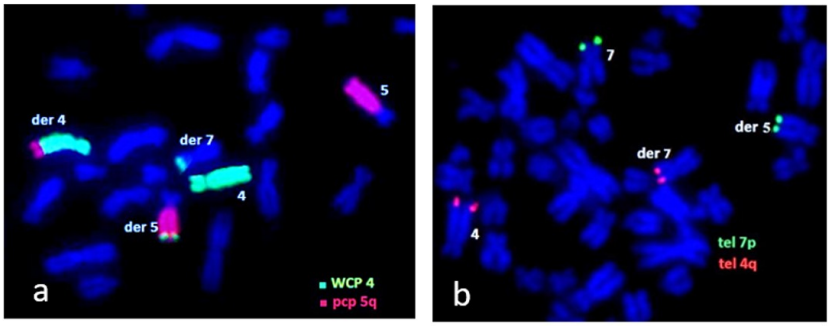

Figure 4. FISH analysis showing derivative chromosomes due to CCR der(4)t(4q;5q)(WCP4+,PCP5q+); der(5)ins(5q;4q)t(5q;7p)(PCP5q+,WCP4q+,tel7p+); der(7)t(4q;7p)(WCP4+). DAPI staining is blue. (a) FISH results with the Whole Chromosome painting (WCP) 4 probe (Green) and Arm Specific Probe (PCP) 5q (Red); (b) FISH results with Sub-Telomere probes for 4q (Green) and 7p (Red).

Furthermore, to determine the possible presence of cryptic imbalances during chromosome rearrangements, we examined DNA from the patient's peripheral blood using CMA. Analysis showed four cryptic interstitial microdeletions associated with the breakpoints on chromosomes 4 and 5: arr[GRCh37] 4q31.23(148822943_150512297)x1,4q32.1q32.2(158325898_163127979)x1,5q31.1(134944147_136148325)x1,5q31.2q31.3(139385563_141214796)x1 (Figure 5).

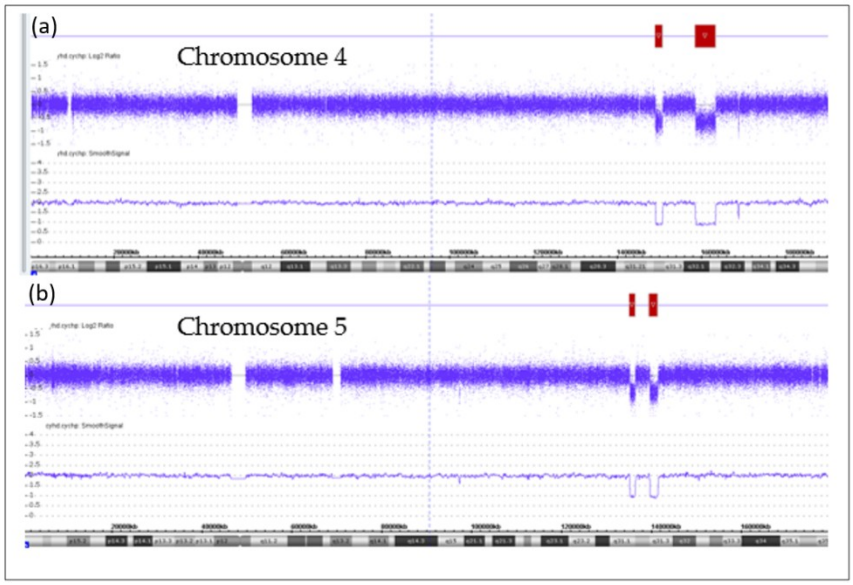

Figure 5. Chromosomal microarray results for chromosome 4 (a) and chromosome 5 (b). The log-2 ratio and smooth signal indicate the deleted regions for both chromosomes 4 and 5.

Notability, that between two microdeletions on derivative chromosome 4 (4q31.3q32.1) and chromosome 5 (5q31.2) there were a disomic region. To clear a question which one of derivative chromosomes contains these regions, we performed a FISH analysis with homemade-labeled probes for this part. We have made two different DNA probes for chromosome 4, one for marking disomic region 4q31.3 which we suspected to see at der(7) nearby Subtelomere 4q (according MCB data) and second for marking 4q32.3 inserted into the derivative chromosome 5. We found that our assumption has approved (Figure 6 a,b).

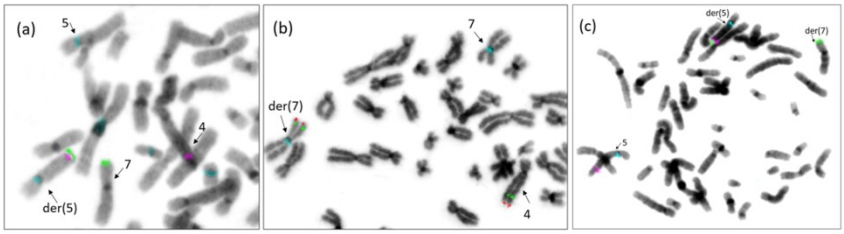

Figure 6. FISH analysis with Homemade labeled Probe. Inverted DAPI staining image. (a) FISH results with CEP 5 (SE 1/5/19) (Blue), Homemade labeled Probe 4q32.3 (Red), Sub-Telomere 7pter (Green); (b) FISH results with CEP 7 (D7Z1) (Blue), Homemade labeled Probe 4q31.3 (Green), Sub-Telomere 4qter (Red); (c) FISH results with Satellite Enumeration Probe (CEP 5) (Blue), Sub-Telomere 7pter (Green) and Homemade labeled Probe 5q31.2 (Red).

FISH analysis for disomic region of chromosome 5 showed the fluorescence signal of 5q31.2 is on the derivative chromosome 5 nearby the subtelomeric 7p signal (Figure 6c). According to previously data FISH analysis, insertional region of chromosome 4 is standing more proximal on derivative chromosome 5. Therefore, we suggest that insertional translocation (5;4)(q31.1;q32q34) is the exact mechanism of the der(5) origin and deletion 5q31.1 was formed due to this event.

DISCUSSION

It has been stated that some apparently balanced translocations are in fact CCRs; some CCRs are more complex than initially expected and could often contain cryptic genomic imbalances (Lee et al., 2010; Guilherme et al., 2013; Campos et al., 2021). Kontodiou et al. (2015) agreed that using chromosome banding alone is insufficient to distinguish between a balanced versus an unbalanced CCR. The application of high-resolution molecular cytogenetic methods, particularly FISH and CMA, are becoming indispensable to detect cryptic imbalances inside or outside of the breakpoint regions. Moreover, Markova et al. (2021) concluded that CMA allowed identifying the unbalanced fragment responsible for occurrence of clinical features in the patient. However, it is impossible to determine a structure of derivative chromosomes using the array data alone. For additional characterization of the chromosomal rearrangement, the FISH analysis necessary with both GTG- analyses and CMA techniques. The apparently balanced chromosomal rearrangements identified in our patient with multiple congenital anomalies and neurodevelopmental abnormalities led us to perform different FISH and microarray analyses, to resolve a nature of the CCR and to find the explanation for her condition.

The present study shows molecular cytogenetic characterization of a *de novo* case, including information about the structure of the CCR and genomic localization of the breakpoints, for a better understanding of the mechanisms involved in CCR formation. We assume three steps of originating a complex rearrangement (Figure 7). First, a balanced translocation 4q;7p produces the microdeletion 4q31.23 at the breakpoint. Evidently, this is followed by insertion of derivative chromosome 7 (material of translocated chromosome 4) into chromosome 5, presumably, with the second microdeletion 4q32.1q32.2 and microdeletion 5q31.1 at the breakpoints. The last step would be a translocation between derivative chromosome 4 and derivative chromosome 5 forming the microdeletion 5q31.2q31.3. Homemade DNA probes for chromosomes 4 and 5 clarified that hypothesis.

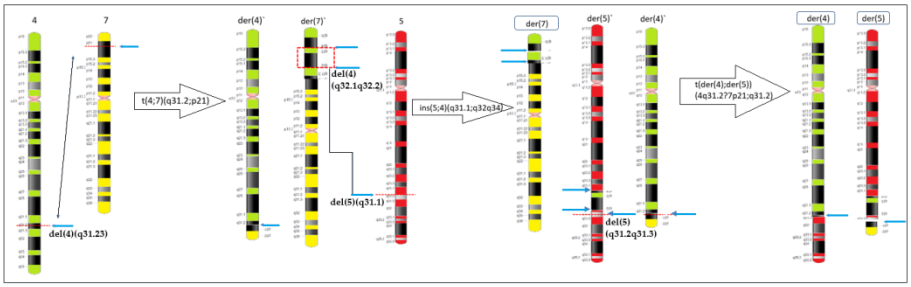

Figure 7. Proposed mechanism of formation of the CCR. Schematic representation of the chromosomes involved in the CCR showing their breakpoints (blue arrows) and four microdeletions detected by CMA.

The combination of cytogenetic, FISH and microarray analysis revealed a complex rearrangement and helped to characterize three derivative chromosomes:der(4)(4pter→4q31.2::5q31.2→5qter);der(5)(5pter→5q31.1::4q32→4q34::5 q31.1→5q31.2→::7p21→7pter);der(7)(4qter→4q34::4q32→4q31.3::7p21→7qter).

Multiple mechanisms could generate these chromosomal rearrangements. Up-to-date few mechanisms have been proposed for chromosomal and genomic recombination, including nonallelic homologous recombination, non-homologous end joining, and fork stalling and template switching (FoSTeS)(Shaffer and Lupski, 2000; Gu et al., 2008; Zhang et al., 2009; Poot and Haaf, 2015). FoSTeS occurs during DNA replication, which is considered the main cause of complex genomic rearrangements, and arguably may have generated these abnormalities in our patient.

In this case CMA revealed a 1,8 Mb and 4,8 Mb microdeletions on chromosome 4 and 1.2 Mb and 1.7 Mb microdeletions on chromosome 5 (Figure 5). The localization of the deletions and correlation of the deleted genes with clinical phenotype are discussed in this report. According to the Genome Data Viewer (https://www.ncbi.nlm.nih.gov/genome/gdv/), the deleted genomic intervals in our patient encompassed more than one hundred genes, including 93 OMIM genes. It is complicated to determine specific genes, loss of functions and their contribution to the phenotypic and neurodevelopmental abnormalities in our patient in this case.

Despite the number and size of CNVs detected by CMA, detailed analysis allowed us to conclude that the main contribution to the clinical phenotype introduced by the deletion 5q31 and gene *PURA (600473)*. Microdeletion within the *PURA* gene with potential activity-dependent roles in neurons encouraged an origin of our patient's abnormal phenotype. The deletion on chromosome 5 encompasses the critical region 5q31 for neurodevelopmental disorders with neonatal respiratory insufficiency, hypotonia, and feeding difficulties. (OMIM#616158). The common cause of this disorder is a heterozygous mutation in the *PURA* gene or PURA syndrome caused by deletions of 5q31.3 occurs to be similarly.

To date, 12 patients (including ours) with 5q31.3 microdeletion syndrome and 85 patients with *PURA* pathogenic variants have been reported (Reijnders et al., 2018; Cinquina et al., 2021). The phenotype of the individuals with 5q31.3 microdeletion syndrome characterized by profound hypotonia, complicated by feeding difficulties, moderate to severe developmental delay/intellectual disability and respiratory difficulties. All these features were noted in our patient. According to literature data, most individuals with *PURA* mutations have abnormal seizure-like movements during the neonatal period. However, like in our patient, EEG monitoring did not show a direct correlation of seizure activity with clinical, abnormal seizure-like events in these cases (Brown et al., 2013). These authors suggested that video-EEG monitoring should form an integral part of the evaluation of abnormal movements in patients with deletion 5q31.3 and Johannesen at al. (2021) considered that PURA-disorder might add to the growing list of developmental and epileptic encephalopathy. Patients with microdeletions 5q31.3 or pathogenic variants in *PURA* have also demonstrated developmental brain changes on MRI, including delayed myelination, white matter abnormalities, widening of the lateral ventricles and the underdeveloped rostrum of the corpus collosum (Lee et al., 2018; Choi et al., 2021).

Other less common clinical manifestations comprise skeletal anomalies (joint hypermobility, scoliosis, congenital hip dysplasia), ophthalmological abnormalities (strabismus, refractive errors), urogenital anomalies (cryptorchidism, kidney stones, congenital hydronephrosis with megaureter, urinary reflux), cardiac malformations (ventricular septal defects, aberrant left subclavian artery, pulmonary stenosis, ductus arteriosus) and endocrine abnormalities (low vitamin D levels) (Reijnders et al., 2018; Cinquina et al., 2021). In our case, previously mentioned malformations were not noted.

Reijnders and joint authors (2018) using computational analysis of facial photographs ascertained that PURA syndrome cases demonstrate core facial dysmorphisms of myopathic face, full cheeks, high anterior hairline, almond-shaped palpebral fissures, and prominent, long philtrum. All of these clinical features were observed in our patient with 5q31.3 microdeletion.

CONCLUSION

Four cryptic microdeletions resulted from this apparently balanced CCR. A combination of distinct approaches helped us to resolve the nature of the patient's CCR, which had an unexpected level of complexity, involving three chromosomes, seven breakpoints, one insertion and four microdeletions. This study demonstrates the necessity of using various cytogenetic and molecular approaches (GTG, FISH with different probes, CMA analysis) to detect hidden rearrangements and to fully characterize the CCR at a precise level. It is very likely that in our patient a de novo 5q31.3 deletion is the main cause for the abnormal phenotype, although other deleted genes certainly contributed to her clinical manifestation; however this is difficult to deteremine in this case.

ACKNOWLEDGMENTS

This research was supported by the State Budget of ICG and by the Ministry of Science and Higher Education of the Russian Federation (#FGFF-2022-0003).

INSTITUTIONAL REVIEW BOARD STATEMENT

The study was conducted according to the guidelines of the Declaration of Helsinki, and approved by the ethical committee of the Research Centre for Medical Genetics (protocol No. 6/2 dated September 14, 2020). Voluntary informed consent was obtained for participation of the patients in this scientific study.

INFORMED CONSENT STATEMENT

Written informed consent was obtained from the patient's parents to be involved in this case report and for the publication of photographs.

CONFLICTS OF INTEREST

The authors declare no conflict of interest.

REFERENCES

Aristidou C, Theodosiou A, Ketoni A, Bak M, et al. (2018). Cryptic breakpoint identified by whole-genome mate-pair sequencing in a rare paternally inherited complex chromosomal rearrangement. *Mol. Cytogenet*. 11: 34. DOI: https://doi.org/10.1186/s13039-018-0384-2.

Brown N, Burgess T, Forbes R, McGillivray G, et al. (2013). 5q31.3 Microdeletion syndrome: clinical and molecular characterization of two further cases. *Am. J. Med. Genet. A.* 161A: 2604-2608. DOI: https://doi.org/10.1002/ajmg.a.36108.

Campos AE, Rosenberg C, Krepischi A, França M, et al. (2021). An apparently balanced complex chromosome rearrangement involving seven breaks and four chromosomes in a healthy female and segregation/recombination in her affected son. *Mol. Syndromol.* 12: 312-320. DOI: https://doi.org/10.1159/000516323.

Choi SA, Lee H-S, Park TJ, Park S, et al. (2021). Expanding the clinical phenotype and genetic spectrum of PURA-related neurodevelopmental disorders. *Brain Dev.* 43: 912-918. DOI: https://doi.org/10.1016/j.braindev.2021.05.009.

Cinquina V, Ciaccio C, Venturini M, Masson R, et al. (2021). Expanding the PURA syndrome phenotype: a child with the recurrent PURA p. (Phe233del) pathogenic variant showing similarities with cutis laxa. *Mol. Genet. Genomic Med.* 9: e1562. DOI: https://doi.org/10.1002/mgg3.v9.110.1002/mgg3.1562.

De Gregori M, Ciccone R, Magini P, Pramparo T, et al. (2007). Cryptic deletions are a common finding in "balanced" reciprocal and complex chromosome rearrangements: a study of 59 patients. *J. Med. Genet.* 44: 750-762. DOI: https://doi.org/10.1136/jmg.2007.052787.

Gu W, Zhang F and Lupski JR (2008). Mechanisms for human genomic rearrangements. *Pathogenetics.* 1: 4. https://doi.org/10.1186/1755-8417-1-4.

Guilherme RS, Cernach MCSP, Sfakianakis TE, Takeno SS, et al. (2013). A complex chromosome rearrangement involving four chromosomes, nine breakpoints and a cryptic 0.6-mb deletion in a boy with cerebellar hypoplasia and defects in skull ossification. *Cytogenet. Genome Res*. 141: 317-323. DOI: https://doi.org/10.1159/000353302.

Higgins AW, Alkuraya FS, Bosco AF, Brown KK, et al. (2008). Characterization of apparently balanced chromosomal rearrangements from the Developmental Genome Anatomy Project. *Am. J. Hum. Genet.* 82: 712-722. DOI: https://doi.org/10.1016/j.ajhg.2008.01.011.

Johannesen KM, Gardella E, Gjerulfsen CE, Bayat A, et al. (2021). PURA-related developmental and epileptic encephalopathy phenotypic and genotypic spectrum. *Neurol. Genet.* 7: e613. https://doi.org/10.1212/NXG.0000000000000613.

Kontodiou M, Daskalakis G, Vetro A, Paspaliaris V, et al. (2015). Complex rearrangement involving three chromosomes, four breakpoints and a 2.7-mb deletion in the 18q segment observed in a girl with mild learning difficulties. *Cytogenet. Genome Res*. 147: 118-123. DOI: https://doi.org/10.1159/000442583.

Lee BH, Reijnders MRF, Abubakare O, Tuttle E, et al. (2018). Expanding the neurodevelopmental phenotype of PURA syndrome. *Am. J. Med. Genet. A.* 176: 56-67. DOI: https://doi.org/10.1002/ajmg.a.38521.

Lee NC, Chen M, Ma GC, Lee DJ, et al. (2010). Complex rearrangements between chromosomes 6, 10, and 11 with multiple deletions at breakpoints. *Am. J. Med. Genet. A.* 152A: 2327-2334. DOI: https://doi.org/10.1002/ajmg.a.33581.

Madan K (2012). Balanced complex chromosome rearrangements: reproductive aspects. a review. *Am J Med Genet A.* 158A: 947-963. DOI: https://doi.org/10.1002/ajmg.a.35220.

Markova ZG, Minzhenkova ME, Bessonova LA and Shilova NV (2021). A new case of 17p13.3p13.1 microduplication resulted from unbalanced translocation: clinical and molecular cytogenetic characterization. *Mol. Cytogenet.* 14: 41. DOI: https://doi.org/10.1186/s13039-021-00562-1.

Pai GS, Thomas GH, Mahoney W and Migeon BR (1980). Complex chromosome rearrangements. Report of a new case and literature review. *Clin. Genet.* 18: 436-444. DOI: https://doi.org/10.1111/j.1399-0004.1980.tb01790.x.

Patsalis PC, Evangelidou P, Charalambous S and Sismani C (2004). Fluorescence in situ hybridization characterization of apparently balanced translocation reveals cryptic complex chromosomal rearrangements with unexpected level of complexity. *Eur. J. Hum. Genet.* 12: 647-653. DOI: https://doi.org/10.1038/sj.ejhg.5201211.

Pellestor F, Anahory T, Lefort G, Puechberty J, et al. (2011). Complex chromosomal rearrangements: origin and meiotic behavior. *Hum. Reprod. Update.* 4: 476-494. DOI: https://doi.org/10.1093/humupd/dmr010.

Poot M and Haaf T (2015). Mechanisms of Origin Phenotypic Effects and Diagnostic Implications of Complex Chromosome Rearrangements. *Mol. Syndromol.* 6: 110-134. DOI: https://doi.org/10.1159/000438812.

Reijnders MR, Janowski R, Alvi M, Self JE, et al. (2018). PURA syndrome: clinical delineation and genotype-phenotype study in 32 individuals with review of published literature. *J. Med. Genet.* 55: 104-113. DOI: https://doi.org/10.1136/jmedgenet-2017-104946.

Riggs ER, Andersen EF, Cherry AM, Kantarci S, et al. (2020). Technical standards for the interpretation and reporting of constitutional copy-number variants: a joint consensus recommendation of the American College of Medical Genetics and Genomics (ACMG) and the Clinical Genome Resource (ClinGen). *Genet. Med.* 22: 245-257. DOI: https://doi.org/10.1038/s41436-019-0686-8.

Shaffer LG and Lupski JR (2000). Molecular mechanisms for constitutional chromosomal rearrangements in humans. *Annu Rev. Genet.* 34: 297-329. DOI: https://doi.org/10.1146/annurev.genet 34.1.297.

Sismani C, Kitsiou-Tzeli S, Ioannides M, Christodoulou C, et al. (2008). Cryptic genomic imbalances in patients with de novo or familial apparently balanced translocations and abnormal phenotype. *Mol. Cytogenet.* 1: 15. DOI: https://doi.org/10.1186/1755-8166-1-15.

Ye J, Coulouris G, Zaretskaya I, Cutcutache I, et al. (2012). Primer-BLAST: A tool to design target-specific primers for polymerase chain reaction. *BMC Bioinformatics*. 13: 134-145. DOI: https://doi.org/10.1186/1471-2105-13-134.

Zhang F, Carvalho CM and Lupski JR (2009). Complex human chromosomal and genomic rearrangements. *Trends Genet.* 25: 298-230. DOI: https://doi.org/10.1016/j.tig.2009.05.005.

